Stellarator-Tokamak Energy Confinement Comparison based on ASDEX Upgrade and Wendelstein 7-X Hydrogen Plasmas

U. Stroth[1,3], G. Fuchert[2], M.N.A. Beurskens[2],
G. Birkenmeier[1,3], P. Schneider[1], E.R. Scott[1,2,4],
K. J. Brunner[2], F. Günzkofer[1,3], P. Hacker[2], O. Kardaun[1],
J. Knauer[2], K. Rahbarnia[2], D. Zhang[2], ASDEX Upgrade team ,
Wendelstein 7-X team , and MST1 team

[1] *Max Planck Institute for Plasma Physics, 85748 Garching, Germany*
[2] *Max Planck Institute for Plasma Physics, 17491 Greifswald, Germany*
[3] *Physik-Department E28, Technische Universität München, 85747*
[4] *Department of Engineering Physics University of Wisconsin–Madison*

September 3, 2020

Abstract

A confinement database with mainly electron-heated hydrogen plasmas from ASDEX Upgrade and Wendelstein 7-X was assembled. Stel-

larator confinement scaling expressions describe both standard discharges in the stellarator and L-mode plasmas in the tokamak similarly well and indicate a similar quality of energy confinement in both devices. While the energy confinement time in ASDEX Upgrade benefits from the smaller aspect ratio of the device, the transport coefficients in Wendelstein 7-X appear to be smaller possibly due to reduced average magnetic field curvature. A physics based confinement scaling is derived from on a model that successfully describes transport in tokamaks. The dimensionally correct scaling has very similar parameter dependencies as the stellarator scalings and reproduces also the trends in the data from ITER L- and H-mode databases reasonably well. On the basis of this scaling, which represents the confinement times of the present data base, average tokamak L-mode and H-mode confinement is 7 % lower and 76 % higher, respectively.

1 Introduction

Energy confinement scaling laws are indispensable tools for the design of fusion experiments and the comparison of the performance of different devices, as is the objective of this work, in which data from stellarators and tokamaks are analyzed. The scaling laws are key to obtaining information about which engineering parameters a system must have in order to reach projected plasma parameters and performance. First scaling expressions [1] were deduced from tokamak data, where the plasma geometry was characterized by major and minor radii, R_0 and a, and the magnetic field by its toroidal component B and the safety factor q_s. Line density $\bar{n}$ and total absorbed

heating power P represented the external control parameters of the plasma. Plasma shaping has a strong impact on global stability and on the linear growth rates of the micro instabilities driving turbulent transport. In order to account for this effect, elongation κ and indentation ϵ were included in the scalings as main parameters to describe the poloidal plasma cross section. In addition there exist individual scaling expressions for the low and high confinement regimes, L- and H-mode, in tokamaks. Since the H-mode is the regime foreseen for future tokamaks such as ITER and possibly DEMO, also current design studies are based on the ELMy H-mode thermal confinement scaling IPB98(y,2) [2]. Consequently, less attention has been paid to L-mode confinement in recent years. The L-mode reference scaling published in 1999 [2] is based on data collected until 1997 [3]. A more recent database from 2006 [4] includes 10 datasets from ASDEX Upgrade and will be used below for comparison.

Plasma shaping is known to affect stability and transport in a complex way. In order obtain robust and practical expressions, however, the confinement time scalings work with log-linear parameter dependencies. This can lead to large uncertainties when extrapolating to parameter values beyond the range covered by the database. Further uncertainties arise from unavoidable correlations, e.g. when a device differs in one parameter from the other devices in the database and at the same time uses a different technique to fuel the plasma or to condition the inner wall, or is equipped with a different wall material. For example, limited reliability of the IPB98(y,2) scaling with respect to operation at high β and Greenwald densities has been identified to affect extrapolations to DEMO [5]. One way to improve the quality of scal-

ings is to restrict the regression to tokamaks which have e.g. similar plasma shapes as the projected device (*step-ladder approach*), as done in Ref. [6].

The present work takes a different route by investigating robust parameter dependencies based as much as possible on physics models. The result is intended to represent the cross-confinement scaling, while the actual confinement of a device can deviate according to specific shaping, wall conditioning, fueling etc. The analysis will combine data from stellarators and tokamaks, devices with very different magnetic configurations, encompassing the Wendelstein 7-AS (W7-AS) dataset used in the ISS95 scaling and recent data from ASDEX Upgrade (AUG) [7] and Wendelstein 7-X (W7-X) [8].

The toroidally asymmetric magnetic configurations of different stellarators cannot be parameterized reasonably with a few parameters. As a virtue of necessity, a first stellarator confinement regression, the ISS95 scaling [9], was done with only 5 parameters, compared to 6–8 used for tokamaks. The main differences being the suppression of the plasma current and the use of an effective plasma radius a_{eff} which is linked to the plasma volume. Further plasma shaping parameters were not used. A later work included stellarator data from the Large Helical Device (LHD) and more recent and improved confinement data from Wendelstein 7-AS. The resulting ISS04 scaling [10] is the present reference for stellarator confinement. While tokamak scalings would have to be rewritten to other parameters when applied to practically current-less stellarators, stellarator expressions can be readily applied to tokamaks and thus allow for direct comparisons. In fact, it was shown that stellarator expressions describe tokamak L-mode confinement reasonably well [11]. Therefore, the other objective of the paper is a first comparison of energy

confinement in stellarators and tokamaks, more explicitly of discharges from AUG and W7-X which are operated at similar parameters.

The paper starts with a description of the database and the definition of parameters used in the regressions. Section 3 describes basic geometric effects on the energy confinement time and compares the devices in the light of an interchange-like transport model. A direct comparison of the data on the basis of established scaling expressions can be found in Sec. 4, and Sec. 5 introduces a physics based scaling expression which is used to compare the data with the ITER confinement databases. Section 6 concludes the paper.

2 Regression parameters and database

Only two variables are used here in the regressions to describe the plasma geometry, the major and the effective minor plasma radii R_0 and $a_{\rm eff}$, respectively. Using $a_{\rm eff}$ as minor radius of a torus with circular cross-section, the plasma volume and separatrix surface area of the actual tokamak are reproduced,

$$V = 2\pi^2 R_0 a_{\rm eff}^2; \quad S = 4\pi^2 R_0 a_{\rm eff}. \tag{1}$$

Besides the plasma geometry, the radial profile of the rotational transform $\iota(r)$ is the main difference between the advanced stellarators W7-AS and W7-X and tokamaks. The ι profiles are flat in both stellarators with values around 1 in the case of W7-X and 1/3 or 1/2 in W7-AS. As in Ref. [9], also in the present work, the rotational transform profile of tokamaks is approximated

by

$$\iota(\rho) = (1 - (1 - \rho^2)^4)/(\rho^2 q_a), \tag{2}$$

where the edge value of the safety factor q_a is taken at the flux surface enclosing 95 % of the toroidal magnetic flux. This simple relation is used to calculate $\iota_{2/3}$, the value of the rotational transform at a normalized radius of $\rho = 2/3$ which is used as regression variable. Although it is physically reasonable to use the safety factor at an intermediate radius rather than at the edge, the relation will not reproduce the actual q values of different discharges and tokamaks equally well and therefor introduces some systematic errors, as discussed below.

The database evaluated here comprises 114 datasets from the stellarator W7-X and 109 from the divertor tokamak AUG. All data are from stationary discharge phases where the plasma conditions in the two devices were as similar as possible. In order to reduce statistical fluctuations, the data was averaged over at least 50 ms. The magnetic field strength is $B \approx 2.5$ T and the working gas is hydrogen in all datasets. Most phases were solely with central electron cyclotron resonance heating (ECRH), only some of the AUG discharges were additionally heated by neutral beam injection (NBI) while the total power was limited to stay in L-mode. The global energy confinement times were derived from the energy content (diamagnetic loop measurement for the stellarators and from MHD equilibra for AUG) and the total absorbed heating power. While the absorption of ERCH power is close to 100 % the NBI power was corrected for shine through, charge-exchange, orbit and ripple losses; also the power absorbed in the scrape-off layer was subtracted. The

database covers the accessible density range where radiation losses are mostly small. A number of 26 W7-X plasmas has a high radiation fraction between 50 and 100 % of the input power. Most of this radiation comes from the scrape-off layer; when the radiation level approaches 100 %, the radiation zone shifts radially inwards to around the last closed flux surface [12]. When normalised to a stellarator scaling expressions, no systematic degradation of the confinement time with the radiative power loss fraction is observed. This has also been reported in Ref. [13]. For this reason, these data were retained in the database. Besides the configuration, the main difference between AUG and W7-X lies in the wall material, which is tungsten in AUG and carbon in W7-X.

The database has been completed by the inclusion of the 250 W7-AS datasets from ISS95 scaling study. This data is from ECRH and NBI heated plasmas at two magnetic field strengths (1.25 and 2.5 T), two values of the rotational transform ($\iota \approx 1/3$ and $1/2$), and an effective minor radius which was varied by movable limiters from 0.11–0.18 m. W7-AS data are from discharges in hydrogen and deuterium. The latter were not removed since the data didn't show an isotope effect, meaning that when isotope mass was added as regression variable the improvement in the fit was negligible. More details are available from Tb. 1 in Ref. [9]. The W7-AS dataset covers the parameter space rather well and thus has a strong impact on the parameter dependencies in the regression analyses. In particular, the magnetic field and minor radius dependencies result from parameter variations inside the W7-AS dataset. The addition of the data allows to derive complete scaling expressions. It was also considered meaningful since main features of

the magnetic configurations of W7-AS and W7-X are similar and turbulent transport can be expected to have a common origin. Both configurations have been optimized for small Pfirsch-Schlüter currents and low neoclassical transport. The shape of the plasma resembles a pentagon when viewed from above, with a stronger magnetic field in the corners. This leads to a separation of regions of bad magnetic curvature and trapped particle populations and e.g. to a stabilisation of the trapped electron mode [14, 15].

At the given plasma parameters it is not to be expected that neoclassical transport, which should be more strongly suppressed by design in W7-X, will dominate the global energy confinement [16, 17, 18]. Although neoclassical fluxes can become relevant in a limited radial range in the inner plasma ($\rho \approx 0.3$) [19], they will not substantially affect the total energy content of the plasmas in this database.

Further devices of the ISS04 database were not considered due to their very different magnetic configurations with respect to those of the advanced stellarators. Additional W7-AS data from the ISS04 scaling are not included either, since they represent mainly improved confinement regimes. Some of this data is used in the following for comparisons.

Table 1 summarizes the parameter ranges covered by the database analyzed here. It should be noted that according to Eq. (1) the effective radius of AUG of 63 cm is substantially larger than its half minor radius of about 50 cm usually used in confinement regressions. W7-X data differs most from the others in the major radius and rotational transform and will therefore have a significant impact on the scaling with the two parameters. The correlation between the two parameters is partially eliminated by the iota variation in

Device	R_0 (m)	$a_{\rm eff}$ (m)	V (m^3)	A	B (T)	$\iota_{2/3}$	no.
AUG	1.6	0.63	12	2.5	2.3–2.6	0.37–0.57	109
W7-AS	2.0	0.12–0.17	1	13.4	1.3–2.5	0.33–0.50	250
W7-X	5.5	0.51	28	10.8	2.4	0.90	114

Table 1: Mean values and ranges of the geometric and magnetic parameters represented in the database for the different devices. The aspect ration is $A = R_0/a_{\rm eff}$ and the last column gives the number of datasets

the W7-AS dataset.

Figure 1a represents the distribution of the recent data from AUG and W7-X in the power density space. The values of the heating power from the two devices fall in the same range from 0.5 to about 4 MW. The density values overlap, too; they vary between 2 and 7.5×10^{19} m^{-3} in both cases, while the majority of the W7-X discharges were done at higher densities than on AUG. The AUG data points are located underneath or on the line that represents the expected power-threshold $P_{\rm LH}^{\rm th}$ for AUG plasmas to access H-mode. It is taken from Ref. [20] and has the form[1]

$$P_{\rm LH}^{\rm H} = 5.18 - 1.09\,\bar{n}_{19} + 0.12\,\bar{n}_{19}^2 \quad \text{for} \quad 2 < \bar{n}_{19} < 6. \tag{3}$$

This fit is only valid in the indicated range of line averaged density $\bar{n}_{19}$. At high density, more power in AUG would trigger a transition to H-mode. The high power values at low density are outside the validity range of Eq. (3). Here the electrons thermally decouple from the ions and the ion heat flux density needed to steepen up the edge ion pressure gradient, which is required to generated the critical radial electric field for a L-H transition, is not reached

[1]Units are MW for power and 10^{19} m^{-3} for density

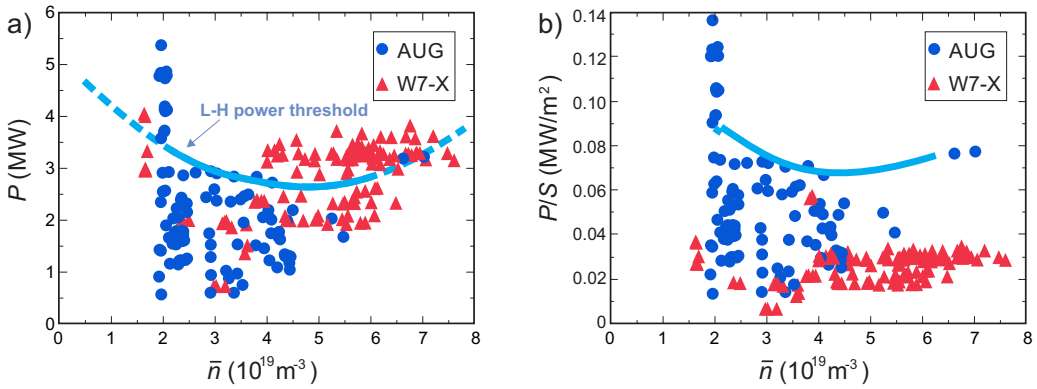

Figure 1: Distribution of the AUG and W7-X data in the plane spanned by total heating power (*left*) and power density crossing the separatrix (*right*) and line averaged density. The lines indicate the power threshold for L-H transitions in hydrogen from Eq. (3) and the one when divided by the separatrix surface area of AUG.

[20, 21]. Figure 1b depicts the total power flux density at the separatrix P/S, which is the relevant quantity to indicate the proximity of the plasma to a L-H transition. For a tokamak, the edge power flux density from W7-X plasmas would be a factor of about three too low to access H-mode. On the other hand, in W7-AS a power of only 200 kW was sufficient to reach H-mode confinement [22]. The corresponding value of $P/S \approx 0.02\,\mathrm{MW/m^2}$ lies also below the L-H transition line in Fig. 1b.

3 Geometrical aspects of global confinement

Next, simple scaling expressions are derived which capture the leading geometrical parameters affecting confinement. This allows disentangling "trivial" changes in confinement due to size and shape of the plasma from those related to changes in the transport coefficients. The original quantities to describe global energy confinement are the different transport coefficients

and the source profiles, from which the radial kinetic density, electron and ion temperature profiles, n and $T_{e,i}$, can be calculated. If the heating power P is deposited in the plasma center and radiation losses can be neglected, the total heat flux through the plasma is radially constant. This links the temperature gradient to the heat diffusion coefficient χ

$$P = -2Sn\chi\nabla T \;\; \Rightarrow \;\; \nabla T = \frac{1}{2Sn}\frac{P}{\chi}, \tag{4}$$

where S is the flux surface area. For the simple estimations here, electron and ion profiles are assumed to be equal. The factor 2 accounts for contributions from both channels. The profiles define the total plasma energy content, which is approximated by the product of characteristic values for density and temperature, $W \approx 3V\bar{n}\bar{T}$. When comparing with data, the rough assumption of $T_e = T_i$ can have an influence on the trends, since temperatures equilibrate more in larger devices. But this variation will be small against those induced by residual dependencies of the diffusivity on the plasma parameters.

Using Eq. (4) and $\nabla T \approx \bar{T}/a_{\mathrm{eff}}$, the energy confinement time gets the form

$$\tau_E = \frac{W}{P} = 3V\frac{\bar{n}\bar{T}}{P} = \frac{V}{S}\frac{3a_{\mathrm{eff}}}{2\bar{\chi}} = \frac{3a_{\mathrm{eff}}^2}{4\bar{\chi}}. \tag{5}$$

For a constant transport coefficient $\bar{\chi}$, the geometry dependence of confinement reduces to a_{eff}^2. The major radius cancels out since both the increase of W by a larger volume V and the higher loss through a larger surface S scale with R_0. The cost of a device scales with magnetic energy and volume.

Expressing the confinement time with Eq. (1) in terms of the volume,

$$\tau_E = \frac{3V}{8\pi^2 R_0 \bar{\chi}} = \frac{3}{4\bar{\chi}} \left(\frac{V}{2\pi^2 A} \right)^{2/3}, \tag{6}$$

highlights the advantage of low aspect ratio devices if only geometrical arguments are used. Under the assumption of the constant values for transport coefficient and plasma volume, a tokamak with an aspect ratio of $A = R_0/a_{\mathrm{eff}} = 2.5$ would be expected to have about 2.5 times higher confinement than a stellarator with $A = 10$. Taking into account the different volumes of AUG and W7-X, but still with a constant values for $\bar{\chi}$, Eq. (6) results in a 1.5 times higher confinement for the tokamak.

This trend can be tested with the present database, where AUG and W7-X are operated at similar heating power, density, and magnetic field strength. Using Eq. (6), values for a mean transport coefficient $\bar{\chi}$ were extracted from the experimental confinement times in the database. Figure 2a depicts the distributions and mean values of the resulting transport coefficients resolved after the different devices. Transport coefficients in the large aspect ratio devices turns out to be substantially lower than in the tokamak. In fact, the geometric disadvantage of a larger aspect ratio is compensated by a reduced transport coefficient. The individual $\bar{\chi}$ values strongly scatter around the means due to variations in the plasma parameters. This is expected since χ is not exclusively determined by geometry but also depends on the plasma profiles which change with power and density.

As a next step, a simple model is introduced to account for the dependence of $\bar{\chi}$ on geometry. Since the plasma parameters are such that neoclas-

sical transport should not play a dominant role, transport is assumed to be turbulent in nature. It can be quantified by the linear growth rates of interchange type of instabilities such as ion temperature gradient (ITG) modes and trapped electron modes (TEM). Their growth rates depend inversely on magnetic field curvature. With the simple ansatz $\bar{\chi} = \chi_0/R_0$, from Eq. (6) results the expression

$$\tau_E = \frac{3V}{8\pi^2\chi_0}, \tag{7}$$

where the energy confinement time becomes independent of plasma geometry.

Again this expression is tested using the database. The result depicted in Fig. 2b shows almost identical mean values of $\chi_0 \approx 7$ for AUG and W7-X. The broad distributions result from the residual dependencies of the transport coefficients on the plasma parameters. Due to the similar parameter ranges in B, n and P, the comparable mean values of χ_0 can be understood as an indication that turbulent transport related to interchange drive, such as ITG modes and TEM, plays a role in the variation of confinement with aspect ratio of the devices. It must be noted, however, that the W7-AS data fit less into that picture.

To close this section, a similar expression is derived for the triple product, where the plasma temperature T is again replaced using Eq. (4). τ_E is given by Eq. (7). If the $1/R_0$ dependence of the transport coefficient holds, the triple product becomes independent of the aspect ratio,

$$nT\tau_E = \frac{3}{32\pi^2}\frac{P}{\bar{\chi}^2}\frac{a_{\mathrm{eff}}^2}{R_0^2} = \frac{3P}{64\pi^2}\frac{V}{\chi_0^2}, \tag{8}$$

and is mainly determined by heating power and plasma volume. In addi-

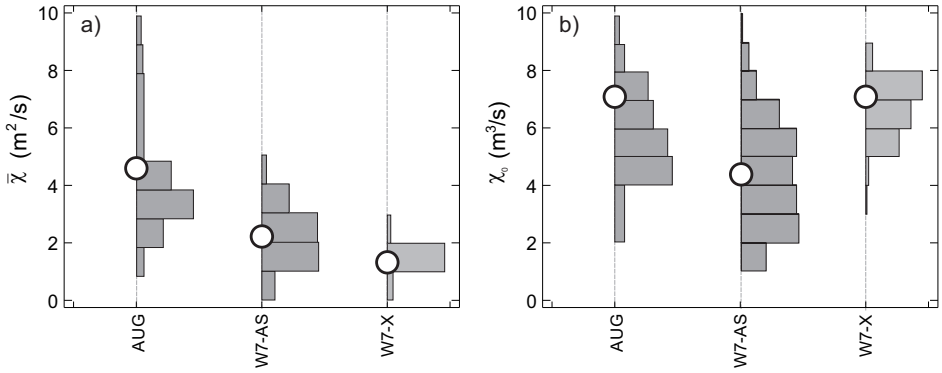

Figure 2: Mean values (*circles*) and distributions in arbitrary units of the mean transport coefficients calculated from Eq. (6) (*left*) and Eq. (7) (*right*) for the different devices. In the plots, the distributions are truncated to values $\bar{\chi} < 10\,\mathrm{m}^2/\mathrm{s}$ but all values are used to calculate the mean values

tion to the simple geometric dependencies discussed here, the value of χ_0 can of course change with plasma shaping. A plasma cross-section optimized for high β will also affect turbulent transport. Related changes of the confinement time will, however, be smaller than the gain in confinement when extrapolating e.g. from AUG to ITER, where the volume increases by a factor of 70. Changes of χ_0 with magnetic field and heating power are probably more important. They will be addressed in the following and a model will be discussed in Sec. 5.

4 Global confinement scaling studies

First, two stellarator scaling expressions are used to analyse the database with emphasis on a stellarator tokamak comparison. Both scalings are rather similar. The ISS95 scaling [9] was derived from data from the advanced stellarator W7-AS and the heliotron/torsatron devices ATF, CHS, and He-

liotron E. Confinement of both stellarator families could be described with the same parameter dependencies, but with an offset in the prefactor. The original ISS95 scaling is defined with a prefactor taken as the mean of the individual prefactors for the two stellarator lines. Since W7-X is an advanced stellarator, it reasonable to use here the ISS95 scaling where the prefactor is used which describes W7-AS confinement:[2]

$$\tau_E^{\mathrm{ISS95_{AS}}} = 0.105\, a_{\mathrm{eff}}^{2.21} R_0^{0.65} P^{-0.59} \bar{n}^{0.51} B^{0.83} \iota_{2/3}^{0.40}. \tag{9}$$

The ISS04 scaling [10] builds on additional data from the heliac TJ-II and the heliotron LHD, a larger device of similar dimensions as W7-X. Furthermore, it includes improved confinement data from W7-AS. The confinement times of the different stellarators were multiplied by individual factors such that their centers of gravity fall onto the ISS95 prediction. The ISS04 scaling has the form

$$\tau_E^{\mathrm{ISS04}} = 0.134\, a_{\mathrm{eff}}^{2.28} R_0^{0.64} P^{-0.61} \bar{n}^{0.54} B^{0.84} \iota_{2/3}^{0.41}. \tag{10}$$

The main difference between the two scalings is the 30 % larger prefactor of the ISS04 expression.

Figures 3a and 3b depict direct comparisons of the database with predictions from the above expressions. It is remarkable how well the $\mathrm{ISS95_{AS}}$ scaling, derived from small devices, describes the confinement time in W7-X, which has an about 30 time larger plasma volume. This strengthens confidence in the predictions of scaling laws. But also the L-mode confinement of the tokamak is rather well reproduced. The alignment of the data with

[2]Units in all scaling expressions are seconds, meter, $10^{19}\,\mathrm{m}^{-3}$, MW, and T.

the ISS04 scaling is of the same quality, the data clouds are only slightly offset. The residues in the logarithmic plots have means and standard deviations of 3.4±6.0 % in case of the $\mathrm{ISS95_{AS}}$ scaling and 10.1±8.9 % for the ISS-04 scaling. For the single devices, the mean experimental confinement times of W7-X are 13 % and 30 % below[3] the $\mathrm{ISS95_{AS}}$ and ISS04 scalings, respectively, while the AUG confinement times are 16 % and 33 % below the respective scaling predictions.

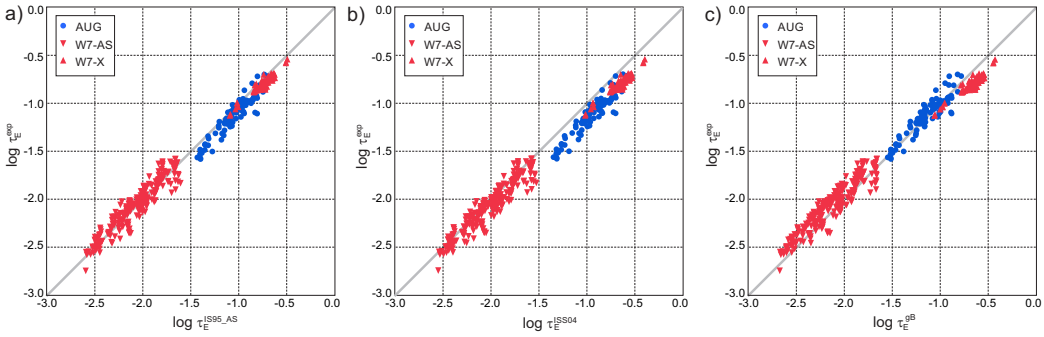

Figure 3: Experimental confinement times from the database compared to the $\mathrm{ISS95_{AS}}$ (9) and ISS04 scalings (10) in (a) and (b), respectively, and (c) to in to the physics-based scaling (14)

The database is not comprehensive enough to derive a scaling reliable in all parameters. However, a free regression of the database leads to the following scaling:

$$\tau_E^{\mathrm{all}} = 0.08\, a^{2.12} R_0^{0.72} P^{-0.60} \bar{n}^{0.50} B^{0.80} \iota_{2/3}^{0.33}, \tag{11}$$

The parameter dependencies are similar to those of the ISS expressions (9) and (10). The errors in the exponents are below 5 %, only for ι it is 15 %. The standard deviation of the regression is 4.7 %, only little lower than for

[3] calculated as the mean of $(\tau_E - \tau_E^{\mathrm{scal}})/\tau_E^{\mathrm{scal}}$ over all respective data points

the $\mathrm{ISS95_{AS}}$ expression. The correlations between the prefactor and both ι and R_0 are rather high. This is because W7-X has at the same time the highest ι value and the largest major radius of all devices. The smaller value of the prefactor is compensated by a higher exponent of R_0. For this reason the use of Eq. (11) for extrapolations is not recommended.

5 Global confinement scaling related to a tokamak heat transport model

In this section, a scaling expression is derived motivated by a critical gradient model for the mean heat diffusivity $\bar{\chi}$ in Eq. (8). Critical gradient models reflect the empirical observation made on tokamaks that electron [23] and ion temperature profiles [24] react stiffly on changes in the power deposition profile. The physical reason for such a behaviour is a threshold in the temperature gradient lengths above which the heat flux induced by ion temperature gradient and trapped electron mode turbulence increases strongly. As a result, the temperature gradient lengths of the profiles stay close to the critical values. The critical-gradient model, of which an element is used here, was proposed in Ref. [25]. The model successfully described electron temperature profiles and transient transport data from different tokamaks and the W7-AS stellarator [26]. Here we refer to the form of Eq. 1 from Ref. [27]. Under the assumption that the temperature gradient lengths of the plasmas in the database are above the critical gradient length by a similar amount, the Heaviside function will be 1 and the heat diffusivity will only scale with

the gyro-Bohm-like leading term of the model [27]

$$\bar{\chi} = \chi^{\mathrm{GB}} \sim \frac{T^{3/2}}{LB^2} q_s^{3/2}, \tag{12}$$

where the safety factor dependency was added ad-hoc to account for the plasma current scaling of tokamak confinement [27]. The electron heat diffusivity in W7-AS was also shown to follow a gyro-Bohm scaling [28]. The inverse dependence on a characteristic length L is consistent with the assumption made in Eq. (7) of interchange-like transport. Here the realistic growth rate dependence on poloidal and toroidal magnetic field curvature is used, $L \sim 1/\sqrt{R_0 a_{\mathrm{eff}}}$, where a_{eff} represents the kinetic pressure scale length. This term might, however, need modifications for specific stellarator magnetic geometries.

Model (12) replaces $\bar{\chi}$ in Eq. (6) with the temperature being expressed in terms of engineering parameters using the second term in Eq. (5). One finds

$$\tau_E \sim V B^2 \iota^{3/2} \left(\frac{a_{\mathrm{eff}}}{R_0}\right)^{1/2} \left(\frac{V\bar{n}}{P\tau_E}\right)^{3/2}. \tag{13}$$

Resolving this expression for τ_E results in a gyro-Bohm like energy confinement scaling of the form

$$\tau_E^{\mathrm{gB}} = 0.089\, a_{\mathrm{eff}}^{2.2} R_0^{0.8} P^{-0.6} \bar{n}^{0.6} B^{0.8} \iota_{2/3}^{0.6}, \tag{14}$$

where the prefactor has been fitted to the database. The similarity of this expression with the ISS scalings (9) and (10) is remarkable. In particular, the dependencies on minor radius, magnetic field strength and heating power

are virtually the same as in (9). Also the prefactor is only about 15 % off. Figure 3c shows that the confinement times of the stellarators and the tokamak in the database align rather well with the above scaling. The increase in the standard deviation compared to that of $\mathrm{ISS95_{AS}}$ in Fig. 3a from 6 to 11 % is moderate. In this representation, the energy confinement in AUG is slightly better than in W7-X. As discussed below, this could be a hint, that due to a lower power flux density through the separatrix (see Fig. 1) in W7-X the edge density and temperature gradients are less developed than in AUG L-mode discharges.

The dependence on rotational transform comes with a larger exponent than in the ISS scalings. For extrapolations, this is not a problem because the values of safety factors and rotational transforms of future tokamak, or stellarator reactors will be similar to those in this database. Due to magnetic islands at rational values, confinement of low magnetic shear stellarators depends in a complicated way on ι [29]. The data in the database comes from standard discharges where the ι profile remains in the vicinity of rational numbers. The $\iota_{2/3}$ values from AUG and W7-AS are in the same range while the value in W7-X is a factor of 2 larger. Therefore a stronger dependence on $\iota_{2/3}$ (0.6 instead of 0.4) penalises the W7-X data in Fig. 3c. The method used to calculate $\iota_{2/3}$ for tokamaks also has a certain degree of arbitrariness that might influence the iota scaling and the device comparison.

The relatively strong density dependence in both the ISS and gB scalings is a more serious issue for extrapolations to stellarator reactor plasmas which can be operated at densities of $2 \times 10^{20}\ \mathrm{m^{-3}}$ or higher. The present data do not support that the $\bar{n}^{0.6}$ dependence remains valid beyond the density range

covered by the database. It was already pointed out in Ref. [9] that a simple exponential fit is not sufficient to reproduce the density dependence of confinement. Similar as in the transition from linear to saturated Ohmic confinement (LOC-SOC) in tokamaks [30], confinement in stellarators increases more strongly with density at low densities, too, while a saturation is indicated at higher density. The same behaviour was also observed on W7-X [13]. Therefore, the use of a moderate density value of e.g. 6×10^{19} m^{-3} is recommended when using the ISS or the gyro-Bohm scaling in extrapolations.

An open issue in this respect is that scaling exponents for the density and heating power comparable to those in Eq. (14) are robustly obtained from cross-machine comparisons, but often do not describe the scaling behavior of τ_E within one experimental device. The reason for this is not yet understood. It could be that cross-machine scalings are more robust against effects that are specific to certain ranges in density and heating power in a particular experiment. But it is also possible that the cross-machine scalings fail to capture important physics elements. Taking them into account could possibly reduce the remaining scatter in the comparisons with data.

While the concept of critical gradients is successful in describing temperature profiles in tokamaks, it can be questioned whether it applies also for the profiles in stellarators. Reference [31] contains a review of profile consistency or resilience – as the effect of critical gradients on temperature profiles was called previously – in stellarators and tokamaks in great detail and points out deviations from profile consistency found on W7-AS. Significant deviations from a resilient electron temperature profile shape occurred in W7-AS if only off-axis ECRH was applied [32]. In later experiments,

however, with an enhanced ECRH system [33], temperature profiles created by different combinations of on- and off-axis ECRH showed clear evidence of profile stiffness [11]. In fact, the same W7-AS electron temperature profiles could be described consistently with a critical-gradient transport model developed for tokamaks [26]. Also on W7-X, indications of stiff ion temperature profiles were found and associated with ITG driven turbulent transport. It can be speculated that the experimentally [34] and theoretically [35] observed toroidal turbulent transport asymmetries in stellarators could, in the flux-surface average, cause a similar transport behavior as in an equivalent tokamak. To conclude this paragraph, it is noted that the concept of critical gradients might also play a major role for stellarator plasmas, as long as turbulence is the dominant transport mechanism.

It is interesting to see how the scaling (14) performs in the context of larger databases. For that reason, Fig. 4a shows a comparison of the gB scaling and confinement times from the present database with the ITER L-mode [4] and ITER H-mode [2, 36] databases. The ITER databases contain data from a large number of tokamaks. Both hydrogen and deuterium discharges are included in the plot. The geometric and magnetic parameters have been translated into stellarator quantities as explained in Sec. 2. Given that the gB scaling is derived from simple arguments and only the prefactor was estimated from the present database, the agreement in both trend and absolute values with the L-mode data (light blue crosses) up to the largest tokamak JET is remarkable. The mean confinement time of the L-mode data is about 7 % below the scaling, which shows that the plasmas in the present database are at good L-mode confinement. The ISS scalings yield a similar

degree of agreement [9]. Also the trend in the H-mode data, which is mostly covered in the plot and only appear in the upper part as pale red plus signs, are described very well by the scaling. The H-mode confinement times are on average about 76 % above the scaling prediction, but they extend mostly parallel to the diagonal line, which indicates that the scaling captures well leading role of geometry for confinement.

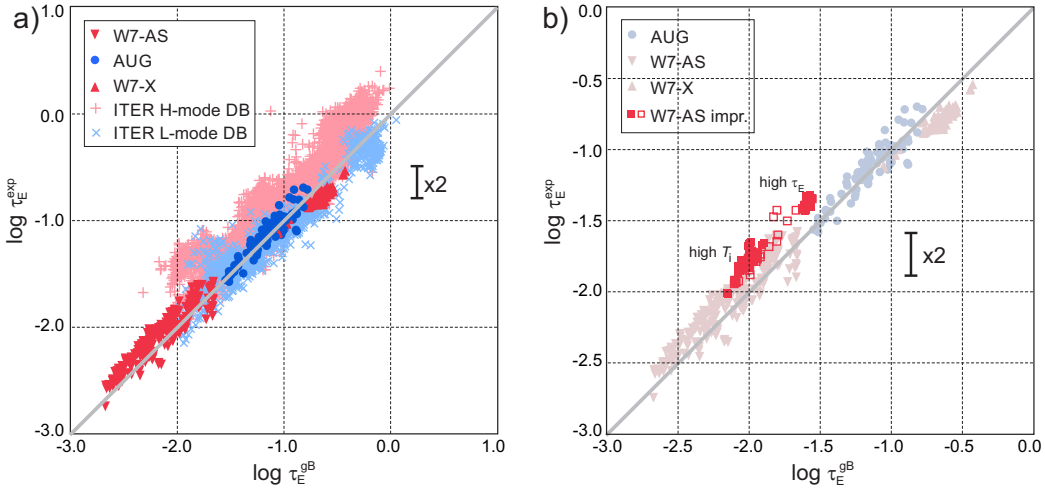

Figure 4: Experimental confinement times from the present database versus the physics-based scaling (14). Data from the ITER L-mode (*light blue*) and H-mode databases (*light red*) are plotted in (a) and additional data from W7-AS discharges with improved confinement (*red squares*) in (b)

For a discussion of the comparison in Fig. 4 it must be kept in mind, that critical transport models describe temperature profiles in tokamaks starting from a boundary value to the core. The outer value is taken approximately at the pedestal top in H-mode plasmas and in L-mode in a similar way at the top of the edge gradient region. Hence, if scaling expression (14) represents core confinement reasonably well, the systematic changes of the edge contribution to the total plasma energy will lead to systematic deviations

from the scaling. The H-mode pedestal brings a gain of up to a factor of about 2 in confinement, leading to the shift of the H-mode data above the scaling prediction in Fig. 4a. A closer inspection reveals that data from individual tokamaks have a systematic offset with respect to the diagonal. This could be a hint to a different pedestal contribution to confinement for the particular device. It is known that e.g. the material of the plasma facing components [37], divertor geometry [38] or plasma shaping [39] can change the H-mode pedestal. The scaling is not designed to account for the contribution of the pedestal, for which a robust scaling model is lacking [40]. Fitting scaling expressions to databases from different devices may, however, produce misleading trends if the mentioned effects on the pedestal shape are cast into dependencies on engineering parameters. In a future study it could be interesting to analyse multi-machine confinement on the basis of an L-mode scaling expression such as (14) and try to relate systematic deviations from the scaling to the confinement regime and the pedestal contribution. Or, similar as attempted in Ref. [41], to combine an L-mode scaling with a scaling expression for the pedestal contribution to the energy content. A more detailed study of systematic deviations of data from different tokamaks from the physics model might give information on the pedestal contribution to confinement, but is outside the scope of this paper.

[41]

Since this work compares stellarator and tokamak confinement, it is important to note that also stellarators can develop improved confinement regimes. The stellarator H-mode – so far clearly observed only in W7-AS – has a moderate effect on confinement of up to 30 % [42]. The high-

confinement data highlighted in Fig. 4b are from W7-AS plasmas with peaked density and peaked ion temperature profiles. In order to control the plasma density, stationary phases were either achieved by combined ECRH and NBI heating (*high* T_i) [43] or with low-power NBI heating only (*high* τ_E) [44]. Confinement during these scenarios is also clearly above the scaling. In the light of recent results from W7-X with transiently improved confinement [18], where peaked density profiles are thought to suppress ITG driven turbulence, the W7-AS high confinement discharges could be interpreted in the same way. While in W7-X pellet injection peaks the density profile, in W7-AS it could have been the lower core fuelling by NBI that caused a suppression of the ITG mode.

6 Summary and conclusions

A direct comparison of the energy confinement in two fundamentally different magnetic configurations has been carried out on a database encompassing AUG and W7-X hydrogen discharges at similar densities and (mostly ECR) heating powers. The database was completed by the W7-AS dataset from the ISS95 database and regressions were done with configuration parameters as they are typically used for stellarators.

A comparison requires a reference, for which established stellarator scaling expressions were used. Without adjusting any parameter, both the $\mathrm{ISS95_{AS}}$ (9) and ISS04 (10) scalings reproduce the global energy confinement time of both stellarators and tokamaks well. In particular, the agreement with the $\mathrm{ISS95_{AS}}$ scaling is excellent. It is remarkable that a scaling deduced

from devices with a typical plasma volume of $1\,\mathrm{m}^3$ predicts confinement in an about 30 times larger device with a deviation of only 11 %. Using this scaling as reference, confinement in W7-X standard discharges is comparable to AUG L-mode confinement. The average confinement time from the ITER L-mode database, where both hydrogen and deuterium data are included, is 7 % below the scaling describing the present data. It was pointed out that with peak density profiles in stellarators and the H-mode in tokamaks regimes with higher confinement are achieved in both devices.

As a second reference, a simple physics based scaling expression was derived. From purely geometric arguments, a lower average heat diffusivity is indicated for W7-X than for AUG. The reduction would be consistent with an $1/R_0$ dependence of an interchange-like transport coefficient. Following this thought, the leading term of a critical gradient model was adopted from the tokamak community. The resulting gyro-Bohm scaling (14), where only the prefactor was fitted to the database, is dimensionally correct and very similar to the ISS expressions. The gyro-Bohm scaling represents the database also with a similar quality and therefore also indicates a similar confinement quality in W7-X standard and AUG L-mode discharges.

The gyro-Bohm scaling describes also the large ITER L- and H-mode databases reasonably well, with of course individual shifts of the centers of gravity of the two datasets. It is argued that the concept of a critical gradient can possibly be applied to tokamaks and stellarators and that deviations from the simple scaling might be related to different contributions of the pedestal to confinement. In a future work it would be interesting to test such an approach on the ITER databases.

Acknowledgement

Helpful discussions with Clemente Angioni and Francois Ryter are gratefully acknowledged. This work has been carried out within the framework of the EUROfusion Consortium and has received funding from the Euratom research and training programme 2014–2018 and 2019–2020 under grant agreement No 633053. The views and opinions expressed herein do not necessarily reflect those of the European Commission.

References

[1] R. J. Goldston, Plasma Phys. Controll. Fusion **26**, 87 (1984).

[2] ITER Physics Basis Expert Groups on Confinement and Transport and Confinement Modelling and Database, ITER Physics Basis Editors, Nucl. Fusion **29**, 2175 (1999).

[3] S. Kaye *et al.*, Nucl. Fusion **37**, 1303 (1997).

[4] The version of the ITER L-mode database used here was provided by O. Kardaun in 2020.

[5] H. Zohm *et al.*, Nucl. Fusion **53**, 73019 (2013).

[6] A. Sips *et al.*, Nucl. Fusion **58**, 126010 (2018).

[7] A. Kallenbach *et al.*, Nucl. Fusion **57**, 102015 (2017).

[8] T. Klinger *et al.*, Nucl. Fusion **59**, 112004 (2019).

[9] U. Stroth *et al.*, Nucl. Fusion **36**, 1063 (1996).

[10] H. Yamada *et al.*, Nucl. Fusion **45**, 1684 (2005).

[11] U. Stroth, Plasma Phys. Controll. Fusion **40**, 9 (1998).

[12] D. Zhang *et al.*, *Proc. of the* 46^{st} *Europ. Conf. on Plasma Physics* (EPS, Milan, 2019), p2.1058.

[13] G. Fuchert *et al.*, Nucl. Fusion **60**, 036020 (2020).

[14] P. Helander, J. H. E. Proll, and G. G. Plunk, Phys. Plasmas **20**, 122505 (2013).

[15] J. H. E. Proll, P. Xanthopoulos, and P. Helander, Phys. Plasmas **20**, 122505 (2013).

[16] G. Fuchert *et al.*, Nucl. Fusion **58**, 106029 (2018).

[17] A. Dinklage *et al.*, Nature Physics **14**, 855 (2018).

[18] S. A. Bozhenkov *et al.*, Nucl. Fusion **60**, 066011 (2020).

[19] N. A. Pablan *et al.*, Phys. Plasmas **25**, 22508 (2018).

[20] F. Ryter *et al.*, Plasma Phys. Controll. Fusion **58**, 014007 (2016).

[21] M. Cavedon *et al.*, Nucl. Fusion **57**, 014002 (2016).

[22] M. Hirsch *et al.*, Plasma Phys. Controll. Fusion **50**, 053001 (2008).

[23] F. Ryter *et al.*, Plasma Phys. Controll. Fusion **42**, A323 (2001).

[24] P. Mantica *et al.*, Phys. Rev. Lett. **102**, 175002 (2009).

[25] F. Imbeaux *et al.*, Plasma Phys. Controll. Fusion **43**, 1503 (2001).

[26] F. Ryter *et al.*, Plasma Phys. Controll. Fusion **48**, B453 (2006).

[27] X. Garbet *et al.*, Plasma Phys. Controll. Fusion **46**, 1351 (2004).

[28] U. Stroth *et al.*, Phys. Rev. Lett. **70**, 936 (1993).

[29] R. Brakel *et al.*, Nucl. Fusion **42**, 903 (2002).

[30] A. Lebschy *et al.*, Nucl. Fusion **58**, 026013 (2017).

[31] F. Wagner and U. Stroth, Plasma Phys. Controll. Fusion **35**, 1321 (1993).

[32] H. J. Hartfuß *et al.*, Plasma Phys. Controll. Fusion **36**, B17 (1994).

[33] V. Erckmann *et al.*, in *Radio Frequency Power in Plasmas*, edited by M. Porkolab and J. Hosea (AIP Conf. Proc., New York: AIP, 1993), No. 289, p. 137.

[34] G. Birkenmeier *et al.*, Phys. Rev. Lett. **107**, 025001 (2011).

[35] P. Helander, Plasma Phys. Controll. Fusion **64**, 124009 (2012).

[36] The version of the ITER H-mode database (DB4V5X) used here was provided by F. Ryter in 2017.

[37] A. Weller *et al.*, Nuclear Materials and Energy **8**, 12 (2017).

[38] H. Q. Wang *et al.*, Nucl. Fusion **58**, 096014 (2018).

[39] T. H. Osborne *et al.*, Nucl. Fusion **42**, A175 (2000).

[40] M. N. A. Beurskens *et al.*, Phys. Plasmas **109**, 18 (2011).

[41] D. McDonald *et al.*, Nucl. Fusion **47**, 147 (2007).

[42] V. Erckmann *et al.*, Phys. Rev. Lett. **70**, 2086 (1993).

[43] M. Kick *et al.*, in *Plasma Physics and Controlled Fusion Research (Proc. 16^{th} Int. Conf., Montreal, Canada, 1996), IAEA, Vienna*, edited by IAEA (IAEA, Vienna, 1997), Vol. 2, p. 27.

[44] U. Stroth *et al.*, Plasma Phys. Controll. Fusion **40**, 1551 (1998).